Tight-binding electrons on triangular and kagomé lattices under staggered modulated magnetic fields: quantum Hall effects and Hofstadter butterflies

2011 J. Phys.: Condens. Matter 23 156002

(http://iopscience.iop.org/0953-8984/23/15/156002)

J. Phys.: Condens. Matter **23** (2011) 156002 (9pp) doi:10.1088/0953-8984/23/15/156002

Tight-binding electrons on triangular and kagomé lattices under staggered modulated magnetic fields: quantum Hall effects and Hofstadter butterflies

Juan Li[1], Yi-Fei Wang[1] and Chang-De Gong[1,2]

[1] Center for Statistical and Theoretical Condensed Matter Physics, and Department of Physics, Zhejiang Normal University, Jinhua 321004, People's Republic of China
[2] National Laboratory of Solid State Microstructures and Department of Physics, Nanjing University, Nanjing 210093, People's Republic of China

E-mail: yfwang_nju@hotmail.com

Received 8 February 2011
Published 1 April 2011
Online at stacks.iop.org/JPhysCM/23/156002

Abstract

We consider the tight-binding models of electrons on a two-dimensional triangular lattice and kagomé lattice under staggered modulated magnetic fields. Such fields have two components: a uniform-flux part with strength ϕ, and a staggered-flux part with strength $\Delta\phi$. Various properties of the Hall conductances and Hofstadter butterflies are studied. When ϕ is fixed, variation of $\Delta\phi$ leads to the quantum Hall transitions and Chern numbers of Landau subbands being redistributed between neighboring pairs. The energy spectra with nonzero $\Delta\phi$s have similar fractal structures but quite different energy gaps compared with the original Hofstadter butterflies of $\Delta\phi = 0$. Moreover, the fan-like structure of Landau levels in the low magnetic field region is also modified appreciably by $\Delta\phi$.

(Some figures in this article are in colour only in the electronic version)

1. Introduction

The integer quantum Hall effect (IQHE), discovered in 1980 [1], is observable in two-dimensional (2D) electron gas systems, at low temperatures and in the presence of a strong perpendicular magnetic field, which splits the electron energy spectrum into discrete Landau levels (LLs). While the Fermi energy lies in the gap between two LLs, the Hall conductance, which for each state can be labeled by the Chern number in units of e^2/h, is accurately quantized to an integer. Landau quantization and disorder-induced localization can well explain the phenomenology of the IQHE. In fact, the precise quantization of the Hall conductance was explained by Laughlin [2] based on a gauge-invariance argument, and further theoretical elaboration was made possible through the picture of edge states by Halperin [3]. However, it is also natural to explain the realization of the IQHE by explicit calculations based upon the linear-response Kubo formula, for periodic systems under a uniform magnetic field [4] and with additional random potential [5–7].

The electronic properties of 2D periodic lattice structures immersed in a uniform magnetic field are of special interest and have been hot topics for many physicists since about 30 years ago when Hofstadter [8] found the energy spectrum to have recursive and fractal structures for a square lattice. The tight-binding electrons on a 2D triangular lattice [9, 10] and kagomé lattice [11, 12] also revealed rich and peculiar physics in the presence of a perpendicular magnetic field. A triangular plaquette is a basic building block of built-in geometrical frustration. The energy dispersion and the density of states on a triangular lattice with uniform magnetic flux have been investigated [13]. The kagomé lattice is a 2D lattice composed of corner-sharing triangles. The kagomé systems have a frustrated ground state which exists at a magnetic field of one-half of a flux quantum per triangular plaquette [12].

For 2D periodic lattice structures, a spatially nonuniform staggered magnetic field is interesting both theoretically and experimentally. For metallic ferromagnets on a particular lattice such as a kagomé one, a fictitious staggered magnetic flux is induced by intrinsic chiral spin orderings or an external

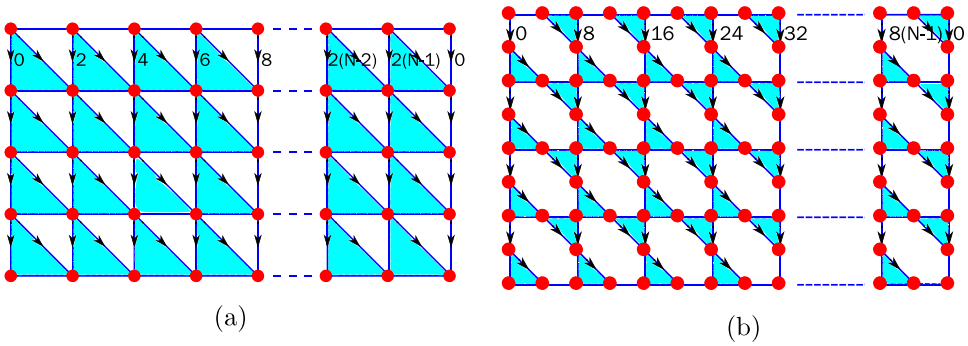

Figure 1. Illustration of the selected gauge on 2D lattices and corresponding PBCs. The number labels represent the gauge phase as multiples of ϕ. Other phase factors are uniquely determined. The shaded triangles indicate the magnetic flux strength, being $\phi + \Delta\phi$. (a) A lattice which is topologically equivalent to a triangular lattice. (b) A lattice that is topologically equivalent to a kagomé lattice, which is made up of triangular and hexagonal plaquettes.

magnetic field [14–16], and gives rise to a special extended Haldane model of quantum anomalous Hall effects [17]. If this spin ordering opens a charge excitation gap, a spontaneous quantum Hall effect will even occur, e.g. in a triangular lattice [18]. Recently, the magnetotransport properties were also investigated for tight-binding electrons on a 2D square lattice in staggered modulated magnetic fields [19, 20]. Although direct experimental observation of staggered-flux state is still difficult in conventional condensed matter systems, discussion of the various properties of ultracold bosonic or fermionic atoms in optical lattices under an artificial staggered flux became very fruitful [21]. Such artificial uniform or modulated magnetic fluxes are also suggested to be created by inducing some sort of asymmetry in the atomic tunneling between the optical lattice sites [20, 22–26], and are feasible as shown by recent experimental advances [27].

In this paper we study the magnetotransport properties of electrons on a triangular and a kagomé lattice under magnetic fields with alternate flux in neighboring plaquettes. In sections 3 and 4, for both infinite 2D triangular and kagomé lattices, our focus is mainly on two physical quantities: the Hall conductance and the energy spectra displayed as Hofstadter butterflies. The calculation of the Hall conductance by the Kubo formula provides us with a tool to uncover new topological quantum phase transitions in various systems with next-nearest-neighbor hopping [10], random potential [7], staggered-flux modulation [19], spin–orbit coupling [28], orbital degeneracy and spatial anisotropy [29], and is also closely related to electronic transport measurements. The Hofstadter butterflies present global structures of energy spectra in a uniform magnetic field [8] or a staggered magnetic field [30], and are suggested to be detected by density profile or momentum distribution profile measurements in various cold-atom systems [22, 25, 31].

2. Formulation

We start from the tight-binding model Hamiltonian on a 2D lattice:

$$H = -t \sum_{\langle i,j \rangle} (\mathrm{e}^{\mathrm{i}a_{ij}} c_i^\dagger c_j + \mathrm{H.c.}), \tag{1}$$

where $c_i (c_i^\dagger)$ is an electron annihilation (creation) operator on site i; in the following the hopping integral $t = 1$ between two nearest neighbors $\langle i, j \rangle$ is used as the unit of energy. In the presence of a magnetic field B, the phase factor a_{ij} resulting from the vector potential $\mathbf{A}$, for hopping processes between two nearest neighboring sites i and j, is given by

$$a_{ij} = \frac{2\pi}{\phi_0} \int_i^j \mathbf{A} \cdot \mathrm{d}\mathbf{l}, \tag{2}$$

where $\phi_0 = hc/e$ is the flux quantum.

The Landau gauge $\mathbf{A} = (0, -Bx, 0)$ adopted for the staggered modulated magnetic field and the corresponding periodical boundary conditions (PBCs) are shown in figure 1. We add bonds between the next-nearest-neighbor sites of the square lattice in only one direction to get one lattice as shown in figure 1(a), and add sites between the nearest-neighbor sites and link the new sites with bonds of the square lattice in only one direction to get another lattice as shown in figure 1(b). These two lattices are topologically equivalent (namely, they can be continuously deformed) to a triangular lattice and a kagomé lattice, respectively [10, 11, 13]. All the physical properties discussed below for tight-binding electrons in two such lattices are also the same as those for a triangular lattice and a kagomé lattice, respectively.

The magnetic flux per plaquette (the summation of a_{ij} along links around a plaquette) is given by $\phi + \Delta\phi$ and $\phi - \Delta\phi$ alternatively in neighboring plaquettes on the triangular lattice. In order to satisfy the PBCs as shown in figure 1(a), $\phi = \frac{p}{2N} \times 2\pi$ (p and $2N$ are coprime integers) measures the uniform-flux strength, $\Delta\phi$ measures the staggered-flux strength, and both are in units of $\phi_0/2\pi$. On the kagomé lattice, the staggered modulated flux per plaquette is $\phi + \Delta\phi$ and $6\phi - 2\Delta\phi$ in neighboring triangular and hexagonal plaquettes, respectively. To satisfy the PBCs in figure 1(b), the uniform-flux strength for the kagomé lattice is given by $\phi = \frac{p}{8N} \times 2\pi$ (p and $8N$ are coprime integers).

After the numerical diagonalization of the Hamiltonian (1), the total Hall conductance for the system at zero temperature ($T = 0$) is calculated through the Kubo

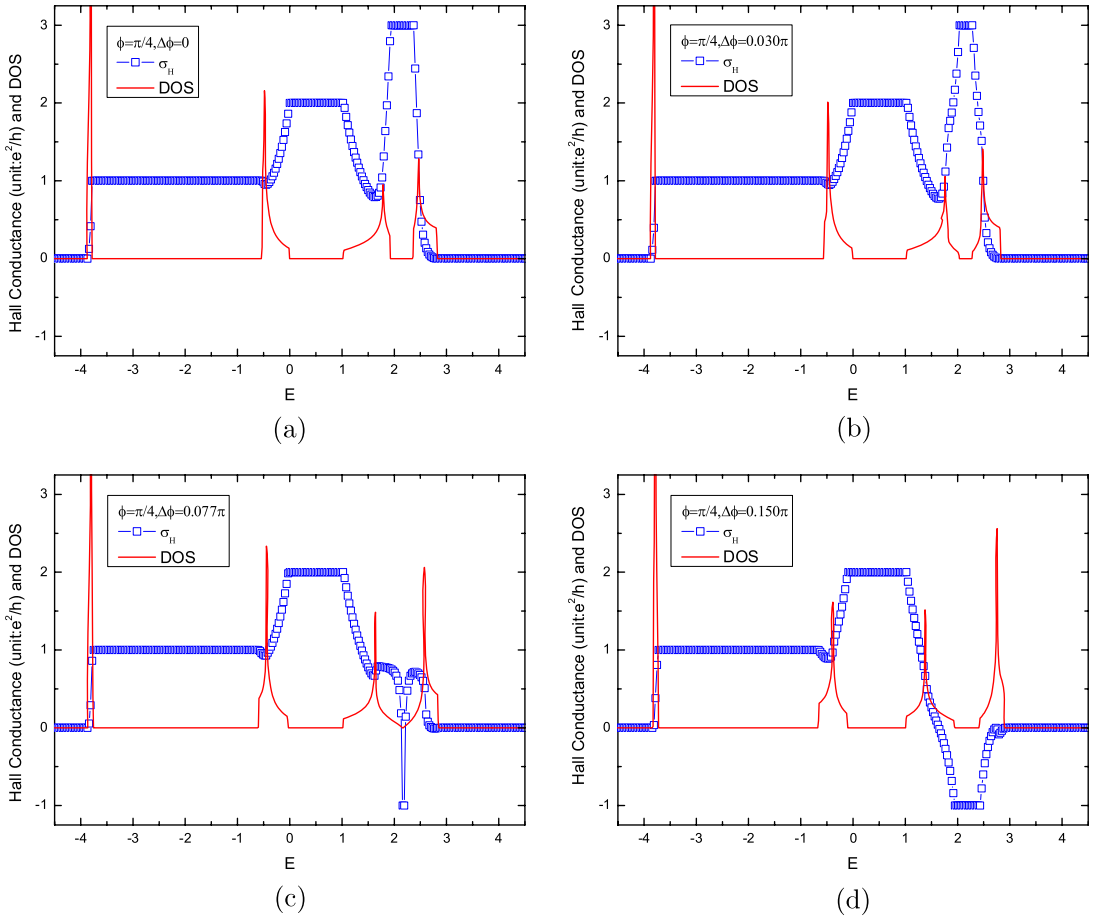

Figure 2. The case with $p = 1$, $N = 4$ for a 2D triangular lattice. The Hall conductance σ_{H} and the DOS versus the Fermi energy E for (a) $\Delta\phi = 0$, (b) $\Delta\phi = 0.030\pi$, (c) $\Delta\phi = 0.077\pi$, (d) $\Delta\phi = 0.150\pi$.

formula [4]:

$$\sigma_{\mathrm{H}}(E) = \frac{\mathrm{i}e^2}{A_0\hbar} \times \sum_{\varepsilon_m<E}\sum_{\varepsilon_n>E} \frac{\langle m|v_x|n\rangle\langle n|v_y|m\rangle - \langle m|v_y|n\rangle\langle n|v_x|m\rangle}{(\varepsilon_m-\varepsilon_n)^2}, \quad (3)$$

where $A_0 = L \times L$ is the area of the system, E is the Fermi energy, ε_m and ε_n are the corresponding eigenvalues of the eigenstates $|m\rangle$ and $|n\rangle$ of the mth and nth Landau subbands. The velocity operator is defined as $\mathbf{v} = (i/\hbar)[H, \mathbf{R}]$ ($\mathbf{R}$ is the position operator of electrons). When E falls in energy gaps, we can rewrite σ_{H} as $\sigma_{\mathrm{H}}(E) = e^2/h\sum_{\varepsilon_m<E} C_m$, where C_m is the Chern number [4] of the mth totally filled Landau subband.

3. Triangular lattice

We first revisit the tight-binding model for a 2D triangular lattice. After the Fourier transformation, an energy dispersion $E(\mathbf{k})$ is given by

$$E(\mathbf{k}) = -2t\left(\cos k_x a + 2\cos\frac{1}{2}k_x a \cos\frac{\sqrt{3}}{2}k_y a\right), \quad (4)$$

where a is the lattice constant and k_x, k_y are two wavevectors in reciprocal space. Equation (4) means that the allowed energies are $-6t \leqslant E \leqslant 3t$ and the bandwidth is $9t$.

3.1. IQHE and phase transition

We consider the case of $p = 1$ and $N = 4$ as an example. The Hall conductance calculated by (3) and the DOS versus the Fermi energy E are shown in figure 2 with uniform-flux strength $\phi = \frac{1}{8} \times 2\pi$ and various strengths $\Delta\phi$s. Because the triangular lattice does not have particle–hole symmetry we therefore have to analyze the full energy region. In figure 2, the Hall conductance σ_{H} and the DOS does not have symmetry about $E = 0$. For the uniform case ($\Delta\phi = 0$), the three IQHE plateaus are well defined with Hall conductance $\sigma_{\mathrm{H}} = le^2/h$, where $l = 1, 2, 3$. The energy gaps between subbands give the widths of these IQHE plateaus. Correspondingly, there are four Chern numbers in sequence, $\{+1, +1, +1, -3\}$.

With $\Delta\phi$ increased from 0 to 0.150π, a systematic evolution of the IQHE plateaus appears. At $\Delta\phi = 0.030\pi$, as can be seen in figure 2(b), there are four well-separated subbands with the corresponding well-defined four sequential Chern numbers $\{+1, +1, +1, -3\}$, and each totally filled subband contributes $\frac{1}{4}$ to the filling factor. At $\Delta\phi = 0.150\pi$ in figure 2(d), a new IQHE plateau $l = -1$ appears and is well defined, and the upper two subbands separate again. Accordingly, the Chern numbers are redistributed as $\{+1, +1, -3, +1\}$. There is a direct transition of the Hall conductance from the $l = 3$ IQHE plateau at the critical filling

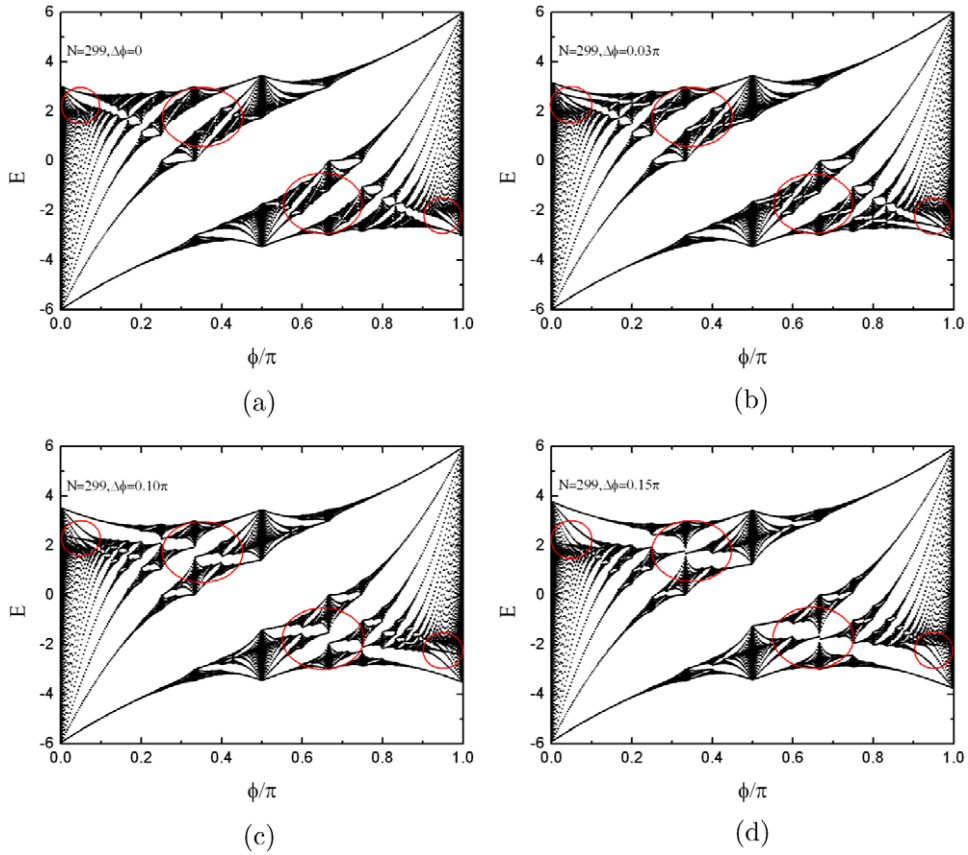

Figure 3. Hofstadter's butterfly for $N = 299$ and various $\Delta\phi$ of 2D triangular lattice tight-binding dispersions in a magnetic field. The value of ϕ/π is p/N, where p satisfies $1 \leqslant p \leqslant N-1$. The solid circles enclose the areas where the spectrum is deformed with various $\Delta\phi$s.

$\nu = \frac{3}{4}$. In figure 2(c), $\Delta\phi$ is increased to 0.077π and the $l = 3$ IQHE plateau disappears. The upper two subbands merge together and form a pseudogap, and their Chern numbers are not well defined due to the lack of an energy gap [4]. Thus $\Delta\phi = 0.077\pi$ is close to the critical point where the transition takes place with a quantized jump from the $l = 3$ IQHE to the $l = -1$ IQHE plateau. When the Fermi energy is pushed higher than $E = 3$, all subbands are completely filled, and the values of the Hall conductance falls back to zero. Through extensive numerical calculations, we find that for other and larger values of N, there always exist such kinds of phase transitions from $l = N-1$ to -1 Hall plateaus.

In the case with $p = 3$ and $N = 4$, both the Hall conductances and the DOS at various $\Delta\phi$s are related to the case with $p = 1$ and $N = 4$ by reversing the direction of the energy axis. At $\Delta\phi = 0, 0.030\pi$, there are four separated subbands with the corresponding four sequential Chern numbers $\{+3, -1, -1, -1\}$. When $\Delta\phi$ increases to 0.077π, the lower two subbands merge together and form a pseudogap. At $\Delta\phi = 0.150\pi$, the lower two subbands separate again and the Chern numbers are redistributed as $\{-1, +3, -1, -1\}$. At $p = 3$ and various N, the Chern numbers have a more complicated redistribution behavior, similar to the square-lattice case [19], revealed by numerical calculations.

3.2. Hofstadter butterflies of energy spectra

For a certain p ($p = 1, 2, \ldots, N-1$), we can obtain all energy eigenvalues ε_ns by numerical diagonalization of the Hamiltonian in (1). The energy spectrum for an infinite 2D triangular lattice is that of the Hofstadter butterfly [8], which is shown in figure 3. We show how the spectrum versus ϕ/π is deformed with various $\Delta\phi$s and the identical $N = 299$. The solid circles enclose the areas in which the spectrum is appreciably deformed when $\Delta\phi$ varies. In Hofstadter's butterfly, we can see many Landau subbands. In the presence of a uniform magnetic field the energy spectrum (as shown in figure 3(a)) lacks either the reflection symmetries with respect to the energy axis $E = 0$ or the $\phi/\pi = 1/2$ axis, in contrast to the square-lattice Hofstadter butterfly because the triangular lattice has no particle–hole symmetry as stated before [9]. However, there is a central symmetry about $\phi/\pi = 1/2$, and clustering patterns of LLs are also obvious. Furthermore, the energy gaps which are characteristic of the Hofstadter butterfly are present in the fractal patterns.

Compared with figure 3(a), figures 3(b)–(d) still have similar fractal structures but the energy gaps are quite different from the original Hofstadter butterfly at $\Delta\phi = 0$, and the global spectral structure becomes deformed. It should be noted that the spectral structure still has central symmetry, and we may focus only on the case of $\phi/\pi \leqslant \frac{1}{2}$. At $\Delta\phi = 0.10\pi$, in

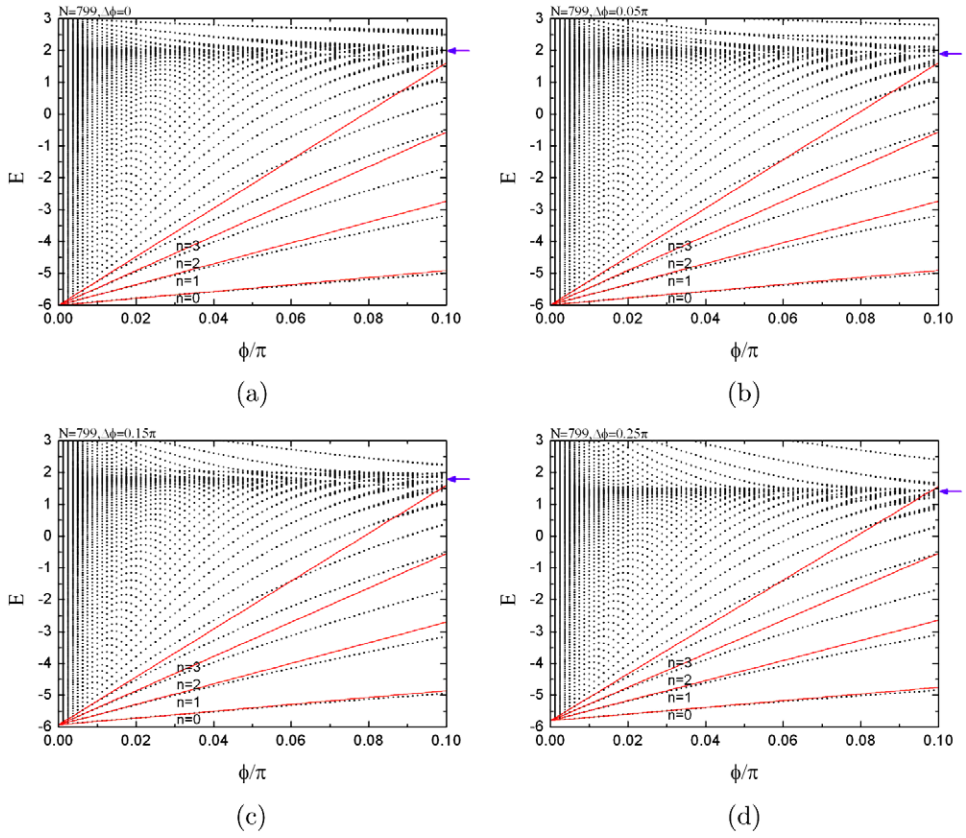

Figure 4. Blowup of Hofstadter's diagram in a uniform magnetic flux for $N = 799$ and different staggered fluxes (a) $\Delta\phi = 0$, (b) $\Delta\phi = 0.05\pi$, (c) $\Delta\phi = 0.15\pi$, (d) $\Delta\phi = 0.25\pi$ on a triangular lattice. The LLs near $E = -6$ are close to linearity. The arrows indicate the position of van Hove singularities.

figure 3(c), a level crossing appears in the gap region of $0 < \phi/\pi < 0.1$ and $2 < E < 2.5$, but it is absent in figure 3(a). Furthermore, new fine structures appear in the original large gap region of $0.25 < \phi/\pi < 0.45$ and $0.5 < E < 3$, when $\Delta\phi$ is increased from 0 to 0.10π and then to 0.15π.

We now consider the LLs at the lower-energy edges for the triangular lattice under a staggered magnetic field $\Delta\phi$. In the presence of a magnetic field, the momentum operator $\mathbf{p}$ is replaced by its gauge-invariant form that includes the magnetic vector potential $\mathbf{A}$:

$$\mathbf{p} \to \Pi = \mathbf{p} + \frac{e}{c}\mathbf{A}. \tag{5}$$

This is called the Peierls substitution, where $\mathbf{A}$ is the vector potential and $\mathbf{B} = \nabla \times \mathbf{A}$. The Hamiltonian is usual

$$H = \frac{(\mathbf{p} + \frac{e}{c}\mathbf{A})^2}{2m}, \tag{6}$$

and the energy levels, for non-relativistic electrons, are

$$E_n = \hbar\omega_c(n + \tfrac{1}{2}), \tag{7}$$

where $\omega_c = eB/(mc)$ is the cyclotron frequency, and (7) represents the non-relativistic LLs.

In the presence of staggered flux only, the tight-binding band for a triangular lattice near the bottom of the dispersion is approximately

$$E(\mathbf{k}) \approx -6t\cos\frac{\Delta\phi}{3} + \frac{\hbar^2}{2m^*}(k_x^2 + k_y^2), \tag{8}$$

with the effective mass $m^* = \hbar^2/(3ta^2\cos\frac{\Delta\phi}{3})$. Hence, the cyclotron frequency is $\omega_c = \frac{4\sqrt{3}t\phi}{\hbar}\cos\frac{\Delta\phi}{3}$.

Therefore the LLs near the bottom of the band can be written as

$$E = t\left[-6 + 4\sqrt{3}\phi\left(n + \frac{1}{2}\right)\right]\cos\frac{\Delta\phi}{3}, \tag{9}$$

in linear order of uniform-flux strength ϕ, and also proportional to $\cos\frac{\Delta\phi}{3}$.

We should notice from figure 3 that the large gaps above the energy $E = -6$ remain. Figure 4 displays a blowup of the low uniform field region and the LLs as a function of ϕ/π. The fan of LLs extends from the origin at $E = -6$ and $\phi/\pi = 0$. When $\Delta\phi = 0$ is increased to $\Delta\phi = 0.25\pi$, the origin of the Landau fan shifts higher than $E = -6$ and obeys (9). The first four LLs and the slopes at small ϕ/π given by (9) are shown in figure 4. The arrows indicate the positions of van Hove singularities. The external uniform magnetic field $\phi/\pi = \frac{p}{799}$ is rather weak, and the energy gaps are also very narrow. In figure 4(a), at $\Delta\phi = 0$, there is an indication of a van Hove singularity around the band $E = 2$ as shown by the arrow.

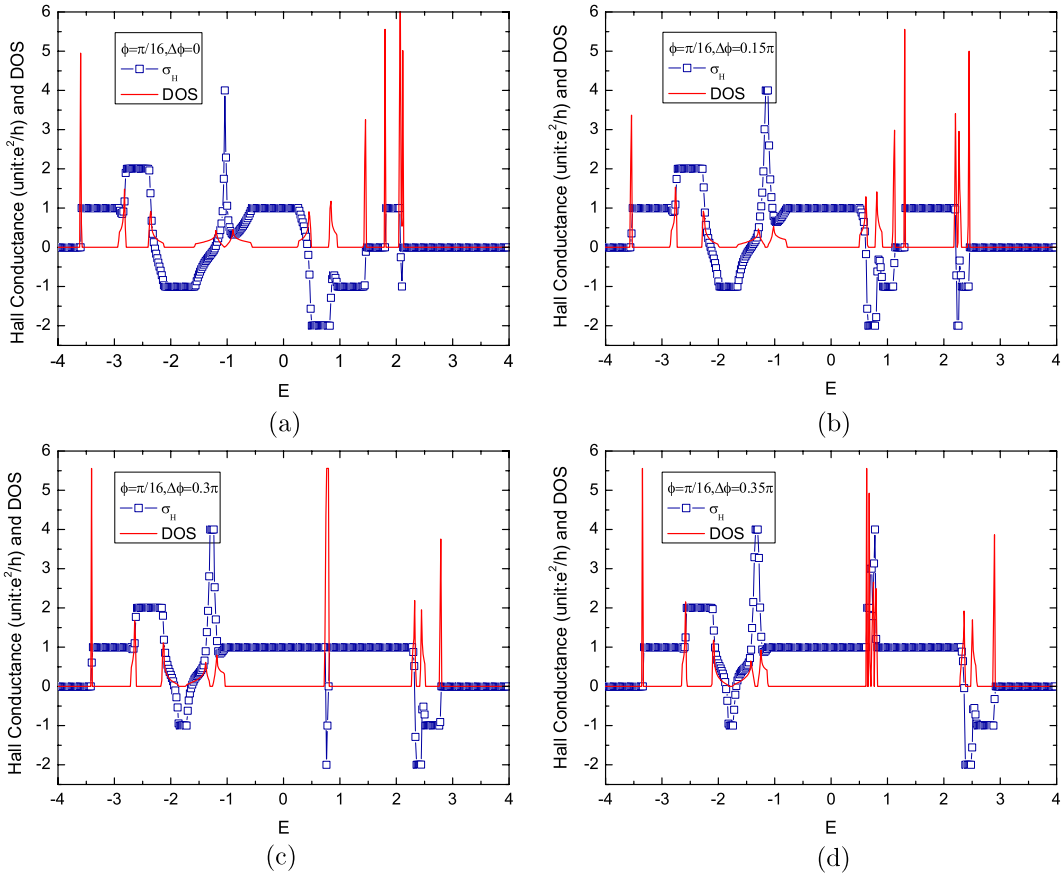

Figure 5. The case with $p = 1$, $N = 4$ for a kagomé lattice. The Hall conductance $\sigma_{\rm H}$ and the DOS versus the Fermi energy E for (a) $\Delta\phi = 0$, (b) $\Delta\phi = 0.15\pi$, (c) $\Delta\phi = 0.3\pi$, (d) $\Delta\phi = 0.35\pi$.

In the presence of a staggered flux, and when $\Delta\phi$ increased to 0.25π, the position of the van Hove singularity shifts gradually to lower energies.

4. Kagomé lattice

Before considering the behavior of electrons on a kagomé lattice under a staggered modulated magnetic flux, we first revisit the tight-binding model of electrons making the nearest-neighbor hops on the kagomé lattice in the absence of a magnetic field. In contrast to a triangular lattice, a kagomé lattice is not a simple Bravais lattice but has three sites per unit cell. Thus after diagonalizing the tight-binding Hamiltonian, we obtain three energy bands:

$$\epsilon_{1,2}(\mathbf{k}) = -t \mp t\sqrt{1 + 8\cos\mathbf{k}\cdot\mathbf{a}_1\cos\mathbf{k}\cdot\mathbf{a}_2\cos\mathbf{k}\cdot\mathbf{a}_3},$$
$$\epsilon_3(\mathbf{k}) = 2t, \tag{10}$$

where $\mathbf{k} = (k_x, k_y)$ is a wavevector in reciprocal space, $\mathbf{a}_1 = \frac{a}{2}(-1, -\sqrt{3})$, $\mathbf{a}_2 = a(1, 0)$, and $\mathbf{a}_3 = \frac{a}{2}(-1, \sqrt{3})$ (a is the lattice constant) denote the three nearest-neighbor vectors. The two dispersive bands ϵ_1 and ϵ_2 contact at the Dirac point $K = (2\pi/3a, 0)$ (or $K' = (\pi/3a, \pi/\sqrt{3}a)$). Close to the $\mathbf{K}$ (or $\mathbf{K}'$) vector, as $\mathbf{q} = \mathbf{k} - \mathbf{K}$, with $|\mathbf{q}| \ll |\mathbf{K}|$, the electrons behave as Dirac fermions with an approximately linear dispersion relation

$$\epsilon_{1,2} = -t \mp v_{\rm F}|\mathbf{q}| + O[(q/K)^2], \tag{11}$$

where $v_{\rm F} = \sqrt{3}at$ is the Fermi velocity and $\mathbf{q}$ is the momentum measured relative to the Dirac points. Thus, except for the flat band ϵ_3, the two dispersive energy bands $\epsilon_{1,2}$ are similar to those in graphene [32]. Later we will make further LL analysis of the energy spectrum around the energy $\epsilon = -1$.

The spectrum of the two low bands (ϵ_1, ϵ_2) ranges over the interval $[-4, 2]$ and the edges of this interval are reached for $\mathbf{k} = 0$. Close to $\mathbf{k} = 0$, the two bands are parabolic at the bottom of the band at $\epsilon = -4$. The two dispersive bands ϵ_1 and ϵ_2 also contact at the 'Dirac point' at energy $\epsilon_1 = \epsilon_2 = -1$. The flat band $\epsilon_3 = 2$ is completely nondispersive, thus this highest-energy state of electrons is localized and highly degenerate. The following electronic properties in an external magnetic field also testify to some of these features.

4.1. IQHE and phase transition

We consider an example with $p = 1$ and $N = 4$. The picture for both the Hall conductance calculated by (3) and the DOS versus the Fermi energy E are shown in figure 5 with the uniform-flux strength $\phi = \frac{1}{32} \times 2\pi$ and various staggered-flux strengths $\Delta\phi = 0, 0.15\pi, 0.3\pi, 0.35\pi$. Just like the triangular lattice, the kagomé lattice also does not

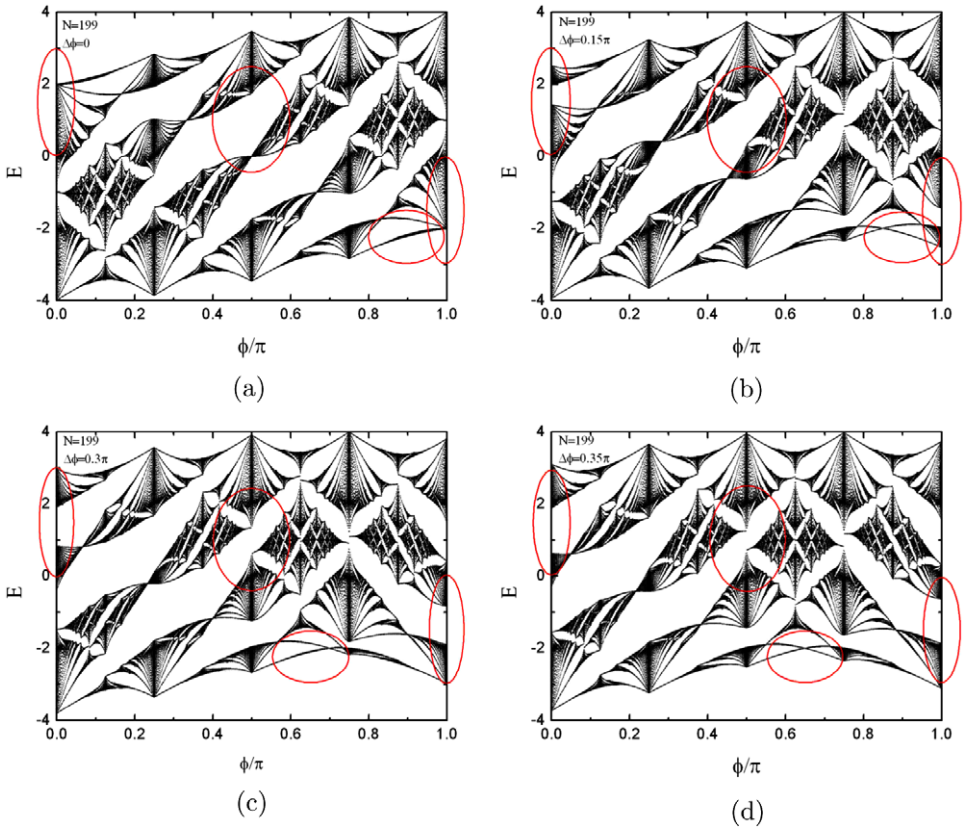

Figure 6. Hofstadter diagram for $N = 199$ and various $\Delta\phi$s of a 2D kagomé lattice in a magnetic field, namely (a) $\Delta\phi = 0$, (b) $\Delta\phi = 0.15\pi$, (c) $\Delta\phi = 0.3\pi$, (d) $\Delta\phi = 0.35\pi$. The value of ϕ/π is $p/4N$ (p are integers), where $1 \leqslant p \leqslant 4N - 1$. The solid circles enclose the areas in which the spectrum is appreciably deformed when $\Delta\phi$ varies.

have particle–hole symmetry. In figure 5, the Hall conductance σ_{H} and the DOS does not have the symmetry about $E = 0$. When $\phi = 0$, the higher band becomes dispersionless [$E_{\mathrm{higher}}(\mathbf{k}) = 2 = \text{const.}$], so after introducing the uniform magnetic field, namely $\phi = \pi/16$, $\Delta\phi = 0$, there should be 12 subbands while the highest three subbands are hard to discern from each other, illustrated by the DOS in figure 5(a). The LLs also exhibit approximate degeneracy near the original flat-band energy $E = 2$. The 10 well-defined IQHE plateaus with the Hall conductance $\sigma_{\mathrm{H}} = l\frac{e^2}{h}$ are also clearly shown in figure 5(a), where $l = 1, 2, -1, 4, 1, -2, -1, 0, 1, -1$. Correspondingly, there are 11 Chern numbers in sequence as $\{+1, +1, -3, +5, -3, -3, +1, +1, +1, -2, +1\}$.

With $\Delta\phi$ increased to 0.15π, the DOS have 12 clearly observable peaks, and among those peaks there are 11 plateaus with Hall conductance $\sigma_{\mathrm{H}} = l\frac{e^2}{h}$ ($l = 1, 2, -1, 4, 1, -2, -1, 0, 1, -2, -1$) and 12 LLs in figure 5(b). Each original band, including the higher-energy flat band, has been split into four LLs when the staggered flux is increased to $\Delta\phi = 0.15\pi$. The Chern numbers are redistributed as $\{+1, +1, -3, +5, -3, -3, +1, +1, +1, -3, +1, +1\}$.

At $\Delta\phi = 0.35\pi$, the DOS also have 12 peaks and there are 11 plateaus and 12 LLs (figure 5(d)). The $l = -2, -1, 0$ IQHE plateaus around the energy $E = 1$ for the case $\Delta\phi = 0.15\pi$ disappear and are replaced respectively by $l = 2, 3, 4$, and the corresponding four peaks of the DOS are very close. The sequential Chern integers are redistributed as $\{+1, +1, -3, +5, -3, +1, +1, +1, -3, -3, +1, +1\}$. In figure 5(c) $\Delta\phi = 0.3\pi$, the four separated peaks for the case $\Delta\phi = 0.15\pi$ merge together into one peak near the energy $E = 0.8$, whereas this peak splits again into four discernible peaks when $\Delta\phi$ increased to 0.35π. So $\Delta\phi = 0.3\pi$ is close to the critical point where the transition from the $l = -2, -1, 0$ IQHE plateaus, respectively to the $l = 2, 3, 4$ IQHE plateaus, takes place and the Chern numbers also redistribute. All the values of the Hall conductances fall back to zero when the Fermi energy is pushed higher than $E = 3$, since all the subbands are completely filled.

4.2. Hofstadter butterflies of energy spectra

The Hofstadter spectrum of the kagomé lattice reveals much richer fractal structures than the triangular and square lattices do. The hierarchical series of energy gaps exist as shown in figure 6. We show that the spectrum versus ϕ/π is deformed with varying $\Delta\phi$ for the kagomé lattice, where $\phi/\pi = \frac{1}{4\times199}p$ ($p = 1, 2, \ldots, 4N-1$), and we label the solid circles enclosing the areas in which the spectrum is appreciably deformed when $\Delta\phi$ varies. In figure 6(a), like the triangular lattice when only the uniform magnetic field is present, the kagomé lattice Hofstadter butterfly also has a central symmetry about $\phi/\pi = \frac{1}{2}$. At $\phi/\pi = 0$, the spectrum ranges over the interval $[-4, 2]$, while at $\phi/\pi = 1$, the energy interval is reversed to $[-2, 4]$.

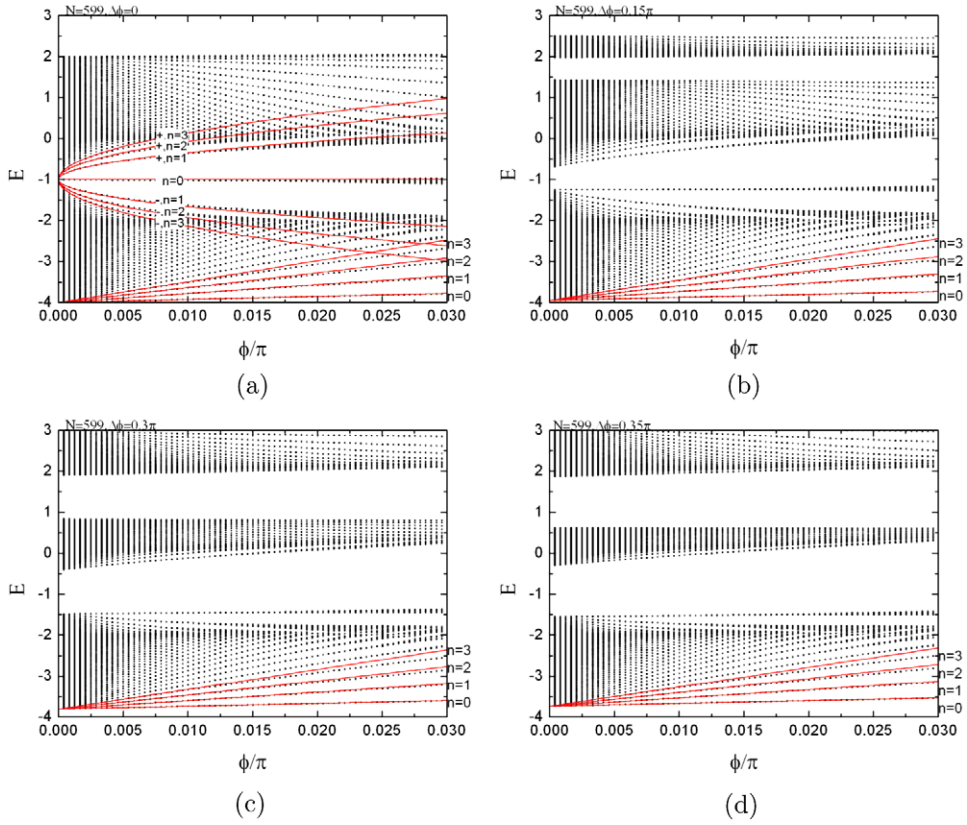

Figure 7. Energy spectrum for LLs in a weak uniform magnetic flux $\phi/\pi = \frac{p}{2396}$ and different staggered fluxes (a) $\Delta\phi = 0$, (b) $\Delta\phi = 0.15\pi$, (c) $\Delta\phi = 0.30\pi$, (d) $\Delta\phi = 0.35\pi$ on a kagomé lattice. The small ϕ/π behavior of the LLs corresponding to $n = 0, 1, 2, 3$ near $E = -4$ is indicated by solid lines. The parabolic lines near $E = -1$ indicate the LL obtained from the Dirac dispersion in a small uniform magnetic field ($\Delta\phi = 0$).

A large spectrum gap appears in the energy interval $[0, 2]$ at $\phi/\pi = 1$.

With increasing $\Delta\phi$, the spectrum still has similar fractal structures but the overall spectrum is deformed in comparison with that in figure 6(a). Besides, the central symmetry is lost about $\phi/\pi = \frac{1}{2}$ in the presence of nonzero staggered flux $\Delta\phi$s (figures 6(b)–(d)). The energy intervals of these spectra also vary with a nonzero $\Delta\phi$ value: at $\phi/\pi = 0$, the minimum of the lower band is larger than the original value -4, and the maximum of the upper band is larger than the original value 2.

The details of the variations in the topology of the Hofstadter diagram with increasing $\Delta\phi$ are self-evident from figure 6.

As for the triangular lattice, we now turn to analyze the LLs for a 2D kagomé lattice under the staggered magnetic flux $\Delta\phi$. We first consider the LLs at the lower-energy edges. When a magnetic flux is introduced, $\mathbf{p}$ is replaced by the Peierls substitution (5). Near the bottom of the kagomé lattice dispersion under the staggered magnetic flux is approximately

$$E(\mathbf{k}) \approx -4t\cos\frac{\Delta\phi}{3} + \frac{\hbar^2}{2m^*}(k_x^2 + k_y^2), \tag{12}$$

with the effective mass $m^* = \hbar^2/(2ta^2\cos\frac{\Delta\phi}{3})$. Hence, the cyclotron frequency is $\omega_c = \frac{8t\phi}{\sqrt{3}\hbar}\cos\frac{\Delta\phi}{3}$.

The LLs near the bottom of the band can be written as

$$E = t\left[-4 + \frac{8\phi}{\sqrt{3}}\left(n + \frac{1}{2}\right)\right]\cos\frac{\Delta\phi}{3}. \tag{13}$$

The lowest LL is linear in ϕ, and also proportional to $\cos\frac{\Delta\phi}{3}$, which is similar to the triangular lattice.

We then start to analyze the case of the LLs around $\epsilon = -1$ on a kagomé lattice in a low uniform magnetic field. The momentum operator $\mathbf{p}$ also is replaced by the Peierls substitution (5). Thus, near $K = (2\pi/3a, 0)$ the bands have the linear dispersion $\epsilon_{1,2}(\mathbf{q}) = \mp v_F|\mathbf{q}|$. The approximate Hamiltonian around one Dirac point can be written in the form

$$H = \begin{pmatrix} 0 & v_F(\Pi_x - i\Pi_y) & 0 \\ v_F(\Pi_x + i\Pi_y) & 0 & 0 \\ 0 & 0 & 2t \end{pmatrix} = \begin{pmatrix} 0 & \sqrt{2}\frac{\hbar v_F}{l_B}a & 0 \\ \sqrt{2}\frac{\hbar v_F}{l_B}a^\dagger & 0 & 0 \\ 0 & 0 & 2t \end{pmatrix}, \tag{14}$$

where the ladder operators $a = \frac{l_B}{\sqrt{2}\hbar}(\Pi_x - i\Pi_y)$ and $a^\dagger = \frac{l_B}{\sqrt{2}\hbar}(\Pi_x + i\Pi_y)$, and we have chosen appropriate normalization factors to obtain $[a, a^\dagger] = 1$, $l_B = \sqrt{\frac{\hbar c}{eB}}$. Therefore, the level

spectra are given by

$$\epsilon_{\mp,n} = \mp\frac{\hbar v_F}{l_B}\sqrt{2n} = \mp 2t\sqrt{2\sqrt{3}\phi n}, \tag{15}$$

namely, the LLs around $K = (2\pi/3a, 0)$ follow

$$E_{\mp} = t[-1 \mp 2\sqrt{2\sqrt{3}\phi n}], \tag{16}$$

where $n = 0, 1, 2, \ldots$. are the quantum numbers of the LLs, and (16) is the so-called 'relativistic' LL around $\epsilon = -1$. The LLs at another Dirac point $K' = (\pi/3a, \pi/\sqrt{3}a)$ have exactly the same spectrum, and hence each LL is doubly degenerate.

Figure 7 show the energy spectrum for the LLs in weak uniform magnetic fields with strength $\phi/\pi = \frac{p}{2396}$. The conventional Landau fan extends to the origin of $E = -4$ and $\phi/\pi = 0$ and with $\Delta\phi$ increased from $\Delta\phi = 0$ to 0.35π; we can also see that the origin of the Landau fan shifts higher than $E = -4$ and obeys (13) as shown by figures 7(a)–(d). The LLs at small ϕ/π are in accordance with the formula (13) (which is illustrated by the solid lines $n = 0, 1, 2, 3$ in figure 7(a)). For the case with $\Delta\phi = 0$ (figure 7(a)), the parabolic lines are clearly seen near the energy $E = -1$, indicating the relativistic-like LL obtained previously from the Dirac dispersion. These relativistic-like LLs are well fitted by (16) $E_{\mp} \propto \mp\sqrt{\phi n}$ ($n = 0, 1, 2, \ldots$) at small ϕ/π. We label the LLs by their quantum numbers $n = 0, \pm 1, \pm 2, \ldots$. Such electronic properties are quite similar to those in graphene [32]. The levels near the original flat-band energy $E = 2$ are still highly degenerate. With $\Delta\phi$ increased, the structures of the energy gaps around the energy $E = -1$ vary gradually (figures 7(b)–(d)).

5. Summary

We have studied both the energy spectrum and the magnetotransport properties of tight-binding electrons on a 2D triangular lattice and kagomé lattice under staggered modulated magnetic fields, with emphasis on the Hall conductance and energy spectra displayed as Hofstadter butterflies. The calculation of the Hall conductance by the Kubo formula uncovers plentiful topological quantum phase transitions. The Hofstadter butterflies provide global structures of energy spectra in such staggered modulated fields. When ϕ is fixed and $\Delta\phi$ is increased from 0 to critical values $\Delta\phi_c$s, the Chern numbers of the Landau subbands will be redistributed between neighboring pairs. The energy spectra for the 2D triangular lattice and kagomé lattice with $\Delta\phi$s have similar fractal structures but quite different energy gaps compared with the original Hofstadter butterflies of $\Delta\phi = 0$. Moreover, the fan-like structure of LLs in the low magnetic field region is also modified appreciably by $\Delta\phi$. Since the staggered flux in both lattices triggers rich quantum Hall transitions and alters the structures of global energy spectra, it is expected these results will stimulate both theoretical and experimental studies on other similar condensed matter or optical lattice systems under spatially modulated real or artificial magnetic fields.

Acknowledgments

This work was supported by the National Natural Science Foundation of China (no. 10904130), and the State Key Program for Basic Researches of China (nos 2006CB921802 and 2009CB929504).

References

[1] Klitzing K V, Dorda G and Pepper M 1980 *Phys. Rev. Lett.* **45** 494
[2] Laughlin R B 1981 *Phys. Rev.* B **23** 5632
[3] Halperin B I 1982 *Phys. Rev.* B **25** 2185
[4] Thouless D J, Kohmoto M, Nightingate M P and den Nijs M 1982 *Phys. Rev. Lett.* **49** 405
[5] Liu D Z, Xie X C and Niu Q 1996 *Phys. Rev. Lett.* **76** 975
[6] Yang K and Bhatt R N 1996 *Phys. Rev. Lett.* **76** 1316
[7] Sheng D N and Weng Z Y 1997 *Phys. Rev. Lett.* **78** 318
Sheng D N and Weng Z Y 1998 *Phys. Rev. Lett.* **80** 580
[8] Hofstadter D R 1976 *Phys. Rev.* B **14** 2239
[9] Claro F H and Wannier G H 1979 *Phys. Rev.* B **19** 6068
[10] Hatsugai Y and Kohmoto M 1990 *Phys. Rev.* B **42** 8282
[11] Yu S L, Li J X and Sheng L 2009 *Phys. Rev.* B **80** 193304
[12] Xiao Y, Pelletier V, Chaikin P M and Huse D A 2003 *Phys. Rev.* B **67** 104505
[13] Hasegawa Y, Lederer P, Rice T M and Wiegmann P B 1989 *Phys. Rev. Lett.* **63** 907
[14] Ohgushi K, Murakami S and Nagaosa N 2000 *Phys. Rev.* B **62** 6065
[15] Katsura H, Nagaosa N and Lee P A 2010 *Phys. Rev. Lett.* **104** 066403
[16] Green D, Santos L and Chamon C 2010 *Phys. Rev.* B **82** 075104
[17] Haldane F D M 1988 *Phys. Rev. Lett.* **61** 2015
[18] Martin I and Batista C D 2008 *Phys. Rev. Lett.* **101** 156402
[19] Wang Y F and Gong C D 2007 *Phys. Rev. Lett.* **98** 096802
[20] Li F, Shao L B, Sheng L and Xing D Y 2008 *Phys. Rev.* A **78** 053617
[21] Lim L-K, Smith C M and Hemmerich A 2008 *Phys. Rev. Lett.* **100** 130402
Lim L-K, Hemmerich A and Smith C M 2010 *Phys. Rev.* A **81** 023404
[22] Jaksch D and Zoller P 2003 *New J. Phys.* **5** 56
[23] Sørensen A S, Demler E and Lukin M D 2005 *Phys. Rev. Lett.* **94** 086803
[24] Shao L B, Zhu S L, Sheng L, Xing D Y and Wang Z D 2008 *Phys. Rev. Lett.* **101** 246810
[25] Gerbier F and Dalibard J 2010 *New J. Phys.* **12** 033007
[26] Stanescu T D, Galitski V, Vaishnav J Y, Clark C W and Das Sarma S 2009 *Phys. Rev.* A **79** 053639
Stanescu T D, Galitski V and Das Sarma S 2010 *Phys. Rev.* A **82** 013608
[27] Lin Y-J, Compton R L, Perry A R, Phillips W D, Porto J V and Spielman I B 2009 *Phys. Rev. Lett.* **102** 130401
Lin Y-J, Compton R L, Jiménez-García K, Porto J V and Spielman I B 2009 *Nature* **462** 628
[28] Wang Y F, Zhao Y and Gong C D 2008 *Phys. Rev.* B **78** 045301
[29] Wang Y F and Gong C D 2010 *Phys. Rev.* B **82** 113304
[30] Wang Y F and Gong C D 2006 *Phys. Rev.* B **74** 193301
[31] Wang J and Gong J 2008 *Phys. Rev.* A **77** 031405
[32] Castro Neto A H, Guinea F, Peres N M R, Novoselov K S and Geim A K 2009 *Rev. Mod. Phys.* **81** 109